System Dynamics of the Open-Draw With Web Adhesion: Particle Approach

Sverker Edvardsson[1]
e-mail: sverker.edvardsson@miun.se

Tetsu Uesaka[2]
e-mail: tetsu.uesaka@fpinnovations.ca

Department of Natural Sciences,
Engineering and Mathematics,
FSCN,
Mid Sweden University,
S-851 70 Sundsvall, Sweden

In the present work we propose a particle approach, which is designed to treat complex mechanics and dynamics of the open-draw sections that are still present in many of today's paper machines. First, known steady-state continuous solutions are successfully reproduced. However, it is shown that since the boundary conditions depend on the solution itself, the solutions for web strain and web path in the open-draw section are generally time-dependent. With a certain set of system parameters, the nonsteady solutions are common. A temporal fluctuation of Young's modulus, for example, destabilizes the system irreversibly, resulting in the continuous growth of web strain, i.e., break. Finally we exemplify with some strategic draw countermeasures how to prevent a dangerous evolution in the web strain. [DOI: 10.1115/1.3197425]

Keywords: paper machine, web breaks, open-draw, runnability, transient boundary conditions, release point, particle simulation, mechanics

1 Introduction

Web breaks of the paper web in the wet end of a paper machine are a major issue for many of today's paper machines. Several breaks a day are common. A frequent problem area is the open-draw section where the wet paper web is unsupported and runs under tension (Fig. 1). In this section, the paper is stretched by typically 3% within a few milliseconds and thus subject to high strain rates. If the strain in any point exceeds about 4% for a defect-free wet (45% solid content) newsprint sheet, web breaks are likely [1,2]. The possible simultaneous existence of minor defects, damages, or holes might make the maximum strain limit even smaller. The basic understanding of the mechanics and dynamics determining the evolution of web tension is of high interest. For example, as the machine speed increases, centrifugal forces increase due to web curvature. For a moderate increase in the machine speed, simultaneous adjustments occur in take-off angle, release angle, and web curvature to restore steady-state operation of the web (see p. 417 in Ref. [3]). However, at even higher speeds, the stability is not guaranteed, and it is known that there is a very small operating window for the stable machine run [4].

Pioneering works of the open-draw properties were performed already in the 1960s by, e.g., Mardon and co-workers [1,5–8]. Also see references in these papers. Although these models addressed many important aspects of the problem, many simplifications and assumptions were required in order to obtain reasonably simple mathematical expressions. Some examples are that only steady-state situations are treated; the effects of bending stiffness, gravity, and air being neglected. In addition, a straight-line outgoing web geometry was assumed. Some current references within the area are given in Refs. [3,9,10]. Here non-steady-state situations are treated but not without restrictions. A detailed review of the models and their various assumptions was recently given by Ahrens et al. [11]. Some crucial limitations of existing models are the neglection of paper thickness (i.e., bending stiffness and viscous bending interactions), web geometry constraints (e.g., circular path), small web deflections, and uncertainties in the boundary conditions (or release conditions applied). In particular, we feel that the limitation of the boundary conditions is critical since, due to the physical situation, the web release generally depends on the web solution itself. Also, due to the dynamic release conditions, the total length of the paper web needs to be flexible in a realistic study of web dynamics. An extension of the computational approach could therefore be valuable in order to obtain the full time-dependent unconstrained solutions.

In this paper we apply a particle approach to investigate the complex mechanics and dynamics of the open-draw sections of paper machines. This approach may be viewed as an analog to the many-body techniques used in celestial simulations of, e.g., colliding galaxies/planetary systems, and the popular molecular dynamics (MD) method [12]. The application of various particle models in mechanics of materials was recently reviewed [13]. Significant developments of particle modeling in mechanics have been made during the past 2 decades. Examples of this are smoothed particle hydrodynamics (SPH), mesh-free Galerkin methods, and MD. These were recently reviewed in Ref. [14]. The discrete element method (DEM) is an example of these particle methods, which appeared as early as in the late 1970s [15–18]. Particle models are also used extensively to multibody system (MBS) analyses, in automobile system design and simulation [19], and also in computer animation of deformable objects [20,21].

In the present context we model the paper web running in the open-draw section as a one-dimensional beam consisting of a series of masses connected by visco-elastic (Kelvin–Voigt) elements. It has already been shown that in the one-dimensional case, the *N*-body approach faithfully reproduces the continuum limit results [20,22]. This aspect, as well as bending, is provided in the Appendix of the present work. Even in a 2D or 3D case, Etzmuss et al. [20] demonstrated that the continuum results can be obtained under certain conditions of orthotropic symmetry and small deformations. The 2D feature of their particle approach may therefore be useful in a future modeling of the paper web as a 2D continuous material. The goal of the present study is to develop a 1D dynamical system model for the open-draw section.[3] It turns out

[1]Corresponding author.

[2]Present address: FPInnovations PAPRICAN Division, 570 St John's Boulevard, Pointe Claire, QC, H9R 3J9, Canada.

Contributed by the Applied Mechanics Division of ASME for publication in the JOURNAL OF APPLIED MECHANICS. Manuscript received March 10, 2009; final manuscript received June 8, 2009; published online December 11, 2009. Review conducted by Martin Ostoja-Starzewski.

[3]A computer C-code is available on request to sverker.edvardsson@miun.se.

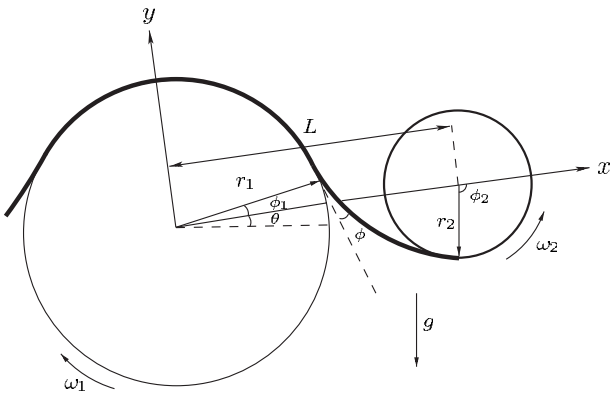

Fig. 1 Model of the open-draw section. Paper web is transferred from the first roll to the second roll. We apply a fixed reference system in the present work.

that the approach is efficient in computation and still captures the essence of the physics taking place on the paper machine.

2 Particle Approach for the System Dynamics

The paper web is here modeled as a series of masses connected by visco-elastic elements. The reference frame (xy) is fixed as shown in Fig. 1, and thus all fictitious forces such as centrifugal and Coriolis forces, etc., are accounted for. We consider only the movements in the xy-plane, which allow us to apply a 1D beam model. The continuous beam is represented by a discrete system consisting of interacting particles (nodes) [20,22]. Given the local mass density ρ_i of the paper web, we can express the mass of particle i as

$$m_i = \rho_i a_0 TW \tag{1}$$

where a_0 is the equilibrium distance between neighboring particles, the paper thickness is T, and the width of the paper web is W. The various interactions acting on particle i consist of both internal and external forces. According to Newton's laws of motion, the change in momentum of particle i is

$$\frac{d\vec{p}_i}{dt} = \sum_k \vec{f}_{ki}^{\,\text{int}} + \sum_k \vec{f}_{ki}^{\,\text{ext}} \tag{2}$$

where the summation over k is performed for internal (material stress) and external interaction forces acting on node i. Time-integrations subsequently lead to its velocity $d\vec{r}_i/dt = \vec{p}_i/m_i$ and then position $\vec{r}_i$ based on the flexible numerical procedure described below. Equivalence of a particle approach to a continuum counterpart is further discussed in the Appendix.

2.1 Richardson Extrapolation Adapted Time-Integration. Given numerical values calculated for several discrete *spatial* grids, repeated Richardson extrapolation can be utilized to obtain the corresponding continuum value [23]. However, the application of repeated extrapolation in the case of discretization in *time* is uncommon, to the author's knowledge. Besides being a convenient method in the present particle approach, it is still expected to be an effective and accurate method also for time-integrations [24]. (Perhaps one of the most efficient integration methods is the *Bulirsch–Stoer* algorithm. This algorithm is based on Richardson extrapolation as well, but is more complex to implement.)

The N-body integrations carried out in the present work include a large number of particles and integration steps. In each step we are interested in projecting the particle system from a certain time t_0 to t_f in an accurate way. We start the integration of particle i by the linear approximation

$$\vec{r}_i(k+1;\Delta t) = \vec{v}_i(k)\Delta t + \vec{r}_i(k)$$

$$\vec{v}_i(k+1;\Delta t) = \vec{a}_i(k)\Delta t + \vec{v}_i(k) \tag{3}$$

First we use an integration time-step Δt for the whole time interval, i.e., $\Delta t = t_f - t_0$, so Eq. (3) needs to be applied only once to obtain, e.g., $\vec{r}_i(t_f;\Delta t)$. Next we use half the integration time-step, so, obviously, Eq. (3) instead must be applied twice to obtain $\vec{r}_i(t_f;\Delta t/2)$. This procedure is then continued successively with smaller discretizations in time resulting in the series

$$\vec{r}_i(t_f;\Delta t),\ \vec{r}_i(t_f;\Delta t/2),\ \vec{r}_i(t_f;\Delta t/4),\ldots$$

for each one of the particles i (and similarly for the velocities). We can now extrapolate each one of the components of the positional and velocity vectors to obtain very accurate estimates of $\vec{r}_i(t_f)$ and $\vec{v}_i(t_f)$ for all the particles. This is accomplished by applying repeated Richardson extrapolations. The implementation in our code is general, so an arbitrary number of extrapolations may be performed. For example, given that we have calculated the series $A_{m,0} = x_i(t_f;\Delta t/2^m),\ m=0,1,\ldots,m_{\max}$, extrapolated values for $n=1,\ldots,m_{\max}$ and $m=n,n+1,\ldots,m_{\max}$ are obtained through recursion

$$A_{m,n} = A_{m,n-1} + \frac{A_{m,n-1} - A_{m-1,n-1}}{2^n - 1}$$

This numerical scheme is known to be fast and to dramatically improve accuracy [25]. Provided that certain correction terms are *regular*, the most accurate quantity is $A_{m_{\max},m_{\max}}$.

2.2 Initial Conditions and Roll Geometry. The present work applies the following initial conditions. In Fig. 1 we show the basic system geometry. A straight paper web path between the rolls is applied as an initial condition. The corresponding release angle of the first roll is $\phi_1 = \alpha$, and the angle of the second roll is then given by $\phi_2 = \pi - \alpha$. For a given roll configuration, it is seen that $\alpha = \arccos[(r_1+r_2)/L]$ and the length of the straight web at $t=0$ becomes $L_w(0) = (r_1+r_2)\tan\alpha$. The equilibrium spacing a_0 between particles (nodes) is given by $a_0 = L_w(0)/(N-1)$, where N is the chosen number of nodes. The particle system then occupies the points at $\vec{r}_i = \vec{r}_0 + i\vec{a}_0,\ i=0,1,\ldots,N-1$, where $\vec{a}_0 = a_0(\sin\alpha, -\cos\alpha)$ and the initial velocities of the nodes are set to $\vec{v}_i = v_i(\sin\alpha, -\cos\alpha)$. The linear expression $v_i = \omega_1 r_1 + i/(N-1) \times (\omega_2 r_2 - \omega_1 r_1)$ is applied.

2.3 Longitudinal Stiffness and Kinematic Viscosity. Given Young's modulus E, Hooke's law reads $f = EWT\Delta L_w/L_w$. Although E is a material constant, the longitudinal stiffness (spring constant) $\lambda \equiv EWT/L_w$ is not, since the longitudinal stiffness λ depends on the length (L_w) of the system. Suppose that the considered material is homogeneous and that we replace the beam with N particles separated with the distance a_0. Then there are $N-1$ springs and $L_w = (N-1)a_0$. The local stiffness is thus given by $\lambda_{\text{loc}} = EWT/a_0 = (N-1)EWT/L_w = (N-1)\lambda$. In the case of a varying E due to variations such as in dryness and in furnish, the local stiffness is given by $\lambda_{ij} = E_{ij}WT/a_0$ where E_{ij} is the local modulus between particles i and j. In such a case one may identify an effective stiffness of the system according to [26]

$$\frac{1}{\lambda} = \sum_{i<j} \frac{1}{\lambda_{ij}} \tag{4}$$

Given the local stiffness values of the system $(\lambda_{ij} = E_{ij}WT/a_0)$ the resulting elastic force $\vec{f}_{ls}$ acting on particle i (Fig. 2) due to longitudinal stiffness alone becomes

$$\vec{f}_{ls} = \lambda_{i-1,i}(|\vec{r}_{i-1} - \vec{r}_i| - a_0)\vec{e}_{r_{i-1}} + \lambda_{i,i+1}(|\vec{r}_{i+1} - \vec{r}_i| - a_0)\vec{e}_{r_{i+1}} \tag{5}$$

where the $\vec{r}$s are positional vectors and, for example, the relative unit vector $\vec{e}_{r_{i+1}}$ points toward node $i+1$ from the central node i.

To model visco-elastic effects, a longitudinal damping is intro-

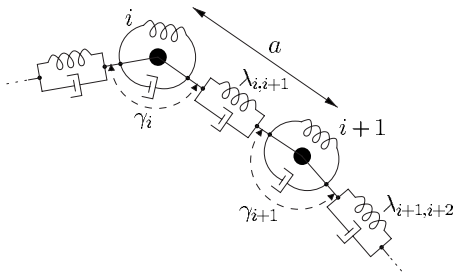

Fig. 2 Topology of a modified Kelvin–Voigt visco-elastic model showing particles interacting through longitudinal stiffness and transverse bending stiffness. Also damping is indicated.

duced in the following way. The moving particle i becomes damped by its neighbors and this force $\vec{f}_{ld}$ is given by

$$\vec{f}_{ld} = -b_{i-1,i}([\vec{v}_i - \vec{v}_{i-1}] \cdot \vec{e}_{r_{i-1}})\vec{e}_{r_{i-1}} - b_{i,i+1}([\vec{v}_i - \vec{v}_{i+1}] \cdot \vec{e}_{r_{i+1}})\vec{e}_{r_{i+1}} \tag{6}$$

where the $\vec{v}$s are velocities and b are phenomenological damping coefficients. For a homogeneous medium, $b=\nu\rho WT/a_0$ where ν is the *kinematic viscosity* and ρ is the mass density for the wet web, i.e., the fiber/water mixture. The special case of bending and its corresponding damping is treated below.

2.4 Bending Stiffness and Viscous Effects. In the short open-draw common in today's paper machines, the bending interactions can become quite significant [11]. We start by considering the local particle system consisting of the nodes $i-1$, i, and $i+1$ in Fig. 3. The local bending potential energy is assumed to be of harmonic form

$$V_i = \tfrac{1}{2}\kappa_i(\gamma_i - \gamma_0)^2 \tag{7}$$

where κ_i is the bending stiffness, γ_i is the bending angle (Fig. 2), and $\gamma_0=\pi$ assuming a planar web at its equilibrium. By definition, a change in potential energy equals the required work dW_i to change the angle from γ_i into $\gamma_i - d\gamma$, see Fig. 3: $-dV_i=\kappa_i(\gamma_i - \gamma_0)d\gamma=dW_i$. By introducing the virtual forces f_{b1} and f_{b2} (useful later in the N-body simulation), the work can also be written as $dW_i=-f_{b1}a_1d\gamma_1-f_{b2}a_2d\gamma_2$, where $d\gamma=d\gamma_1+d\gamma_2$. As we approach the continuum, a good assumption is that $a_1=a_2=a$ and the magnitude of the interactions $f_{b1}=f_{b2}=f_b$. These forces are also orthogonal (indicated in Fig. 3). The system is subjected to restoring forces opposite in the direction acting on each neighboring node ($-\vec{f}_{b1}$ and $-\vec{f}_{b2}$). From the above we have a very good approximation $f_b \approx \kappa_i/a_0(1+\varepsilon)(\gamma_0-\gamma_i)$, where ε is the longitudinal strain in the web. The magnitude of the bending moment for a neighboring node is thus given by $\tau_b=\kappa_i(\gamma_0-\gamma_i)$. Since the two restoring forces $-\vec{f}_{b1}$ and $-\vec{f}_{b2}$ are internal forces, there must also be a force equal in magnitude but opposite in direction, acting on the central node i, i.e., $\vec{f}_{b1}+\vec{f}_{b2}$.

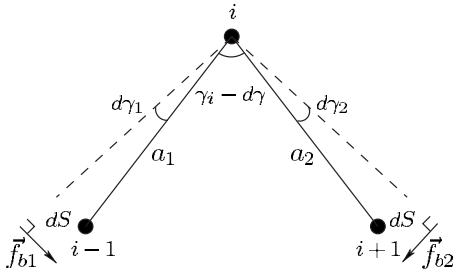

Fig. 3 Elastic bending moment model

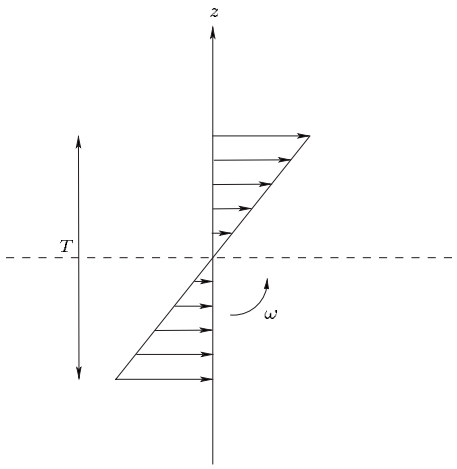

Fig. 4 As the bending web recovers its equilibrium, viscous forces (indicated in the figure) act and tend to damp the restoring movement. The *z*-direction is the normal of the paper web at a given position. In general, this direction varies along the web (fully treated in the present approach).

We shall now apply a beam model in order to determine an estimate of the bending stiffness κ_i. The bending moment τ_b for one of the cross sections of a bent beam is, for a linear elastic material, given by $\tau_b=E_i/R_i\int z^2dA$ (see, e.g., Ref. [27]). The bending radius is R_i and by assuming a smooth variation in Young's modulus it is appropriate to set $E_i=\frac{1}{2}(E_{i-1,i}+E_{i,i+1})$. In the case of a bent paper web with thickness T and width W, $\tau_b=(E_i/R_i)\times(T^3W/12)$, and from the law of cosines for a system as in Fig. 3, $R_i \approx a_0(1+\varepsilon)/2\cos(\gamma_i/2)$. Comparing with $\tau_b=\kappa_i(\gamma_0-\gamma_i)$ and by applying a Taylor expansion around γ_0, we find

$$\kappa_i = \frac{E_i}{a_0(1+\varepsilon)}\frac{T^3W}{12}\frac{2\cos(\gamma_i/2)}{\gamma_0-\gamma_i} \approx \frac{E_i}{a_0(1+\varepsilon)}\frac{T^3W}{12}. \tag{8}$$

This approximation is acceptable because the relative error is still less than 1% as long as the local bending satisfies $|\gamma_0-\gamma_i| < 30$ deg. As we approach the continuum ($\gamma_i \to \gamma_0$), it becomes exact.

Also in the case of damping it is helpful to adopt the approach of a bent beam. As the beam bends, the moment τ_b tends to restore the system to its equilibrium. At the same time there are viscous forces in action slowing down this process. For reasonably small local bending angles, these forces are assumed to be proportional to the angular velocity ω and to the distance z from the *neutral surface*, but opposite in direction (see Fig. 4). The viscous force per unit area (i.e., the cross section of the paper web) is given by $df/dA=(b/WT)\omega z$, and the damping coefficient b is given in Sec. 2.3. The viscous bending moment $d\tau_{vb}=zdf$, so after integration and allowing for a variation in the damping coefficient b, we find

$$\tau_{vb} = b_i\omega\frac{T^2}{12} = \frac{\nu_i\rho_i}{a_0}\omega\frac{WT^3}{12} \tag{9}$$

Given the above viscous moment, the procedure is analogous to the treatment of the bending moment earlier. During the simulation we calculate the angular velocity ω_2 for the right part of the system in Fig. 3. Then we calculate the virtual force $f_{vb}=\tau_{vb}/a_0$ for that node. After this we compute ω_1 for the left node with its corresponding force and, as before, the negative sum of these forces acting on the central node i.

2.5 Estimation of the Adhesion Strength. The adhesion strength may be evaluated differently, depending on the detachment criteria. The one most frequently used is based on Rivlin's

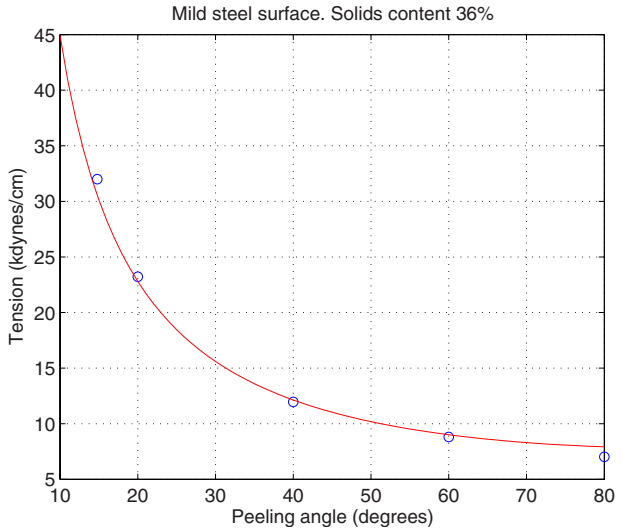

Fig. 5 Tension dependence on peeling angle. A good fit with W_a'=7800 ergs/cm^2 (7.8 J/m^2) is seen. Experimental values indicated by circles from Fig. 19 and Table 6 in Ref. [31].

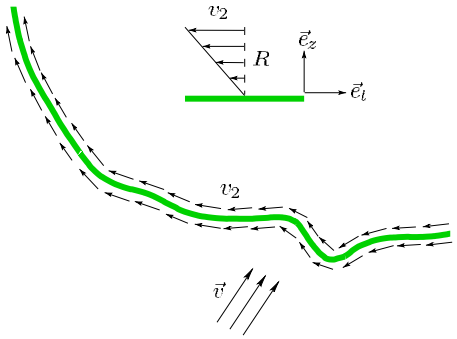

Fig. 6 As the bending web moves through the open-draw, air friction acts on the web elements. The local effect is also indicated. The air speed is set to be the same as in Fig. 1 ($v_2 = \omega_2 r_2$). Also an external perturbation from moving air ($\vec{v}$) is shown.

energy criterion [28]: Detachment occurs when the energy released from the system reaches the work of adhesion, which is regarded as a specific interface material property. Under a quasistatic steady-state condition, which is often used for the experimental determination of adhesive strength, it predicts that

$$T_a = \frac{W_a}{1 - \cos\,\phi_0} \tag{10}$$

where T_a is tension (force per unit width) acting away from the detachment point, ϕ_0 is the angle of the line of action in the experimental setting, and W_a is the work of adhesion (or peeling energy per unit surface). Kaelble [29] showed that Eq. (10) can also be derived by assuming the force couple at the detachment point as the failure criterion. Nicholson [30] noted that the cohesive force criterion also predicts the same angle-dependence as Eq. (10). However, as found by Kaelble [29] and later by Mardon [31] for the wet paper web, Eq. (10) predicts a much steeper angle-dependence of peeling tension than the one that their experimental data showed. To the authors' knowledge there has been no general criterion proposed for the detachment of paper web at different angles.

To obtain an estimate of adhesion strength we shall here simply assume that the detachment occurs when the normal component of resultant force acting on node 0 reaches $a_0 W|\vec{f}_{\text{adh}}(\max)|$ (Fig. 7). Applying this criterion to the quasistatic, steady-state peeling, we predict that

$$T_a W \sin\,\phi_0 = a_0 W|\vec{f}_{\text{adh}}(\max)| \tag{11}$$

The tension may then be written as

$$T_a = \frac{a_0|\vec{f}_{\text{adh}}(\max)|}{\sin\,\phi_0} = \frac{W_a'}{\sin\,\phi_0} \tag{12}$$

This $\sin\,\phi_0$-dependence of tension agreed very well with Mardon's data [31] in a relatively wide angle range, as seen in Fig. 5. Therefore, in this study, we determined $|\vec{f}_{\text{adh}}(\max)|$ from Mardon's data [31] by fitting Eq. (12). It should be noted, however, that Eq. (12) may deviate from the experimental data as the angle exceeds 90 deg.

2.6 Contact Forces, Gravity, and Aerodynamic Effects. In a very dynamic situation the paper web might oscillate and retouch a roll surface. To avoid the penetration of the web within the roll radius r_1 (analogous treatment also for the second roll), a contact interaction was introduced that acts on any node i if its distance $|\vec{r}_i| < 0.99 r_1$. The particular repulsive potential selected here is

$$V_{\text{rep}} = A e^{-r_i/r_1} \tag{13}$$

where r_i is the distance of particle i. If a particle i is near the roll surface ($r_i \approx r_1$), the radial repulsive force becomes $f_{\text{rep}} = (A/r_1)e^{-1}$ and the repulsive parameter A must be high enough to prevent overpenetration. We find that the behavior becomes realistic in magnitude when A is of the same order as f_{ls} (Sec. 2.3). By assuming an appropriate mean stiffness λ, the magnitude $f_{ls} = \lambda(a - a_0) \approx \lambda(\varepsilon a_0) = EWT\varepsilon \sim (A/r_1)e^{-1}$ gives $A = (r_1/e^{-1})EWT\varepsilon$.

The effect of gravity acting on node i is accounted for through

$$\vec{f}_{\text{grav}} = -m_i g(\sin\,\theta, \cos\,\theta) \tag{14}$$

where the machine orientation angle θ is defined between the horizontal line and the x-axis (see Fig. 1).

We also include the effect of air friction (Fig. 6). The friction force per unit area is modeled by $\sigma = \eta du/dz \approx \eta(-v_2/R)$. Here z is the normal direction of the web and η is the viscosity of air (about 18.7×10^{-6} N s/m^2 at 300 K) and R is arbitrarily set to the paper thickness T.

Due to the typical strain variation along the web (Fig. 8), the speed in the majority of the web nodes is v_2. The force on node i then becomes

$$\vec{f}_{\text{fric}} = -2\eta \frac{v_2}{R} a_0 W \vec{e}_t \tag{15}$$

Air resistance may be approximately treated as an external perturbation through standard models where the force for node i is given by

$$\vec{f}_{\text{air}} = \tfrac{1}{2}\rho_{\text{air}} v^2 c_d a_0 W \sin\,\vartheta\,\cos(2\pi\nu t)\vec{e}_v \tag{16}$$

The cosine is introduced to allow simulation of an oscillating pressure with frequency ν. $\rho_{\text{air}} = 1.293$ kg/m^3, v is the speed of the incoming air (Fig. 6), $c_d = 1.17$ for a square plate, and ϑ is the angle of the perturbation relative to the web. More complex air sheet interactions [32–35] are not considered in the present work. Some of these aerodynamic effects could in principle be modeled by adding an effective aerodynamic mass when studying out-of-plane oscillations.

2.7 Conditions of Web Release From the Rolls. Consider the situation in Fig. 7. Before the release of node 0 from the first roll, the strain of the paper web is assumed to be negligible so the distances between these nodes are a_0 (indicated in Fig. 7). The equation of motion is applied only for the nodes $i = 1, 2, \ldots, N-2$ because the nodes 0 and $N-1$ are both fixed to their respective

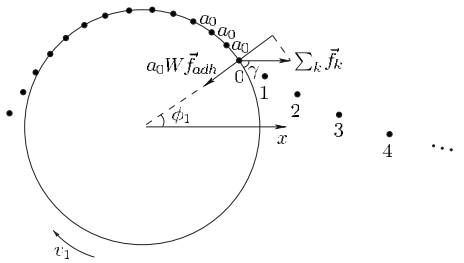

Fig. 7 As the web moves on the first roll, a release occurs each time the sum of the forces exerted on node 0 in the normal direction exceeds the fully developed adhesion force $a_0 W\vec{f}_{adh}(\max)$. If the forces in the normal direction depend on time, the same would be true for the release angle ϕ_1. Since the forces on node 0 depend on the behavior of node 1, which in turn depend on node 2 and so on, the release condition depends on the web solution itself, leading to a complex nonlinear behavior. Also note the possibility of $\gamma \neq \phi$ (Fig. 1).

roll surface. Due to the speed difference $v_2 - v_1$ of the two rolls, the distances between nodes within the open-draw become different from a_0. The release of node 0 (or node $N-1$) is assumed to occur when the normal component of the sum of all forces, i.e., $|\Sigma_k \vec{f}_k| \sin\gamma$ exceeds the magnitude of the maximum adhesion force $a_0 W|\vec{f}_{adh}(\max)|$ (Sec. 2.5). Note that the resultant force $\Sigma_k \vec{f}_k$ is not necessarily along the paper web (Fig. 7), and γ generally differs from ϕ in Fig. 1. The various forces $\vec{f}_k$ acting on 0 contain both elastic and bending forces as well as their corresponding viscous components (Secs. 2.3 and 2.4). We also add the centrifugal contribution to node 0 as well as gravity (Sec. 2.6). The air friction is tangential and does not contribute.

When $|\Sigma_k \vec{f}_k| \sin\gamma > a_0 W|\vec{f}_{adh}(\max)|$, we update the particle system: We create a new node 0 to the left on the roll surface, and the old 0 changes label to 1, and so on: $1 \to 2, 2 \to 3, \ldots, N-1 \to N$. Thus the number of particles in the system is increased by one. Similarly, if a node touches the second roll it is removed from the system, and the number of particles is decreased by one. Also if $|\Sigma_k \vec{f}_k| \sin\gamma > a_0 W|\vec{f}_{adh}(\max)|$ for the node on the second roll, it is reintroduced into the system and the number of particles is increased by one. The adhesion forces for the two rolls can also be set independently. The setup is thus flexible so that the release points are dynamical and the model also avoids imposed constraints in the web geometry such as a circular arc configuration [3,11].

2.8 Transient Release Point and Mass Continuity. Before we proceed to the simulation results, we briefly discuss the steady- to non-steady-state transition in the open-draw system. The web dynamics is generally very complex and time-dependent. Analytical solutions of the complete differential equations are not available. In addition to the general complexity, the fact that the boundary conditions (the release conditions) depend on the solution itself leads to a complex nonlinear behavior.

While the general particle approach in the present work is always time-dependent, there are special cases when the solution becomes stationary. Let us again consider the situation in Fig. 7. Suppose node 0 is released at a certain release angle ϕ_1. The new node 0 is then at the equilibrium distance a_0 away on the roll. Since this node is fixed on the first roll, the time it takes to reach the release point at angle ϕ_1 is exactly given by $\Delta t_1 = a_0/v_1$ where it is released if we have a stationary solution. For the other side of the web at the second roll, the distances between nodes are given by $a = a_0(1+\varepsilon_T)$, where ε_T is the total strain near node $N-1$ (the maximum web strain). The speed of node $N-1$ is exactly v_2 and also node $N-2$ is arbitrary close to v_2 (e.g., in the continuum limit). Thus the time it takes for node $N-2$ to reach the second roll is $\Delta t_2 = a/v_2$. Suppose the operator sets the speed difference of the two rolls according to $v_2 = v_1(1+\varepsilon_{op})$, where ε_{op} is usually called "draw." Then we have

$$\Delta t_2 = \frac{a_0(1+\varepsilon_T)}{v_1(1+\varepsilon_{op})} \tag{17}$$

For stationary cases we have that $\varepsilon_T = \varepsilon_{op}$ (e.g., Eq. 2 in Ref. [9]), so $\Delta t_1 = \Delta t_2$. The number of particles in the system remains constant. In other words, the amount of material entering the system equals the amount exiting the system. This is a necessary condition for a steady-state solution.

Now suppose that we have a situation that introduces a systematic increase in the strain ε_T but the draw ε_{op} is still kept constant. Let us first assume that the release angle ϕ_1 is also kept at a certain constant value. Given a certain curvature, a higher machine speed results in substantially higher centrifugal forces that eventually render the web strain $\varepsilon_T > \varepsilon_{op}$. According to Eq. (17), we see that $\Delta t_2 > \Delta t_1$ and thus the mass balance is lost. The amount of web entering the system is greater than the amount exiting and the steady-state solution is lost. As more and more mass are added to the open-draw section, ε_T increases further through both centrifugal and gravitational contributions. However, since the forces at node 0 are time-dependent, there is no reason why the release angle ϕ_1 should remain constant. In fact, when we remove this restriction and let the release conditions vary, as described in Sec. 2.7, it indeed turns out that $\phi_1 = \phi_1(t)$. What really happens at a high machine speed is that as more webs enter the system the web geometry near node 0 becomes more aligned along the roll surface. Thus the longitudinal force (Sec. 2.3) and the bending force (Sec. 2.4) components in the normal direction of the roll decline (Fig. 7). It is then clear that the release becomes delayed, and, as a consequence, $\phi_1(t)$ will start to move downwards in Fig. 7. This is also seen in the simulations of the present work. Since the release is delayed, $\Delta t_1 = a_0/v_1$ is no longer valid and thus Δt_1 approach Δt_2 (but is still unequal) in its attempt to stabilize the system (self-stabilizing effect).

2.9 Computational Summary. The particle-simulation of the present work is similar to the molecular dynamics simulation technique. Both are started by placing all particles in certain positions and giving them certain initial velocities. The relevant forces (given in Secs. 2.3–2.6) are added up to find the total force acting on each particle. Through Newton's equations of motion, Richardson time-integrations (Sec. 2.1) are employed to compute the changes in the position and in the velocity of each particle during a certain time-step. The integrations are then continued to yield the full dynamics and evolution of the whole particle system.

When the tension normal to the roll surface acting on particle 0 (and similar for $N-1$) exceeds the limit $a_0 W|\vec{f}_{adh}(\max)|$ the web separates from the roll surface. Due to this release condition (Sec. 2.7), the number of particles N in the system becomes flexible. Thus both steady-state and time-dependent solutions (including external perturbations and a dynamic number of particles N) are possible to study. Also as a consequence, the web length L_w is flexible and is time-dependent in many situations.

3 Simulation Results

In this section we first reproduce previous findings of steady-state strain and strain rate in the literature for the purpose of verification. We will also show some typical stationary (steady-state) behavior of the web curvature before we enter the time-dependent and transient web solutions. Unless otherwise stated the following generic *control parameters* are applied in the simulations. They are targeted for wet newsprint (dry basis weight of 45 g/m^2) with 45% dry solid content common in the open-draw section. The estimated mass density $\rho = 1176$ kg/m^3. The thickness of the paper sheet was selected as $T = 100$ μm. The width of

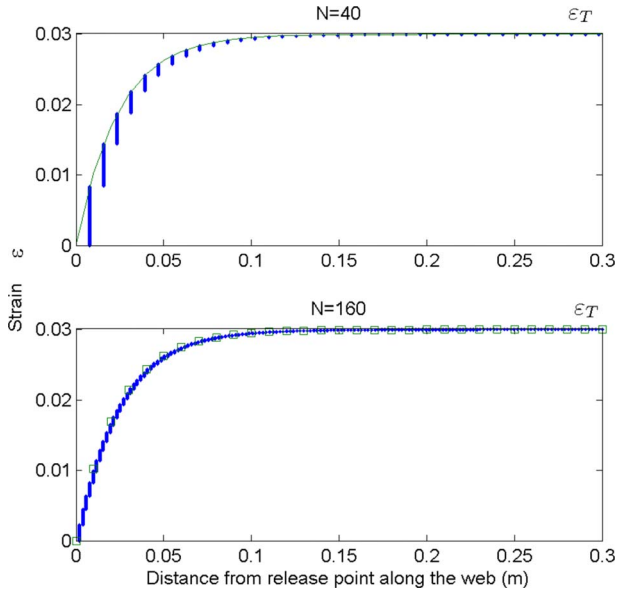

Fig. 8 The stationary strain ε in the open-draw. (Top) The result for $N=40$ nodes. The continuous curve is the continuum solution $\varepsilon(x)$ as given below, where x is the distance from the release point along the web (not to be confused with the x-axis in Fig. 1). (Bottom) The continuum result is essentially obtained for $N=160$ nodes. $\varepsilon(x)$ is plotted here as squares to facilitate comparison. The continuum solution $\varepsilon(x)=(v_2-v_1)/v_1[(1-e^{-kx})/(1-e^{-kL_w})]$, where $k=(E^*-v^2)/\nu v$; $(E^*=E/\rho)$ and $\nu=30$ m^2/s.

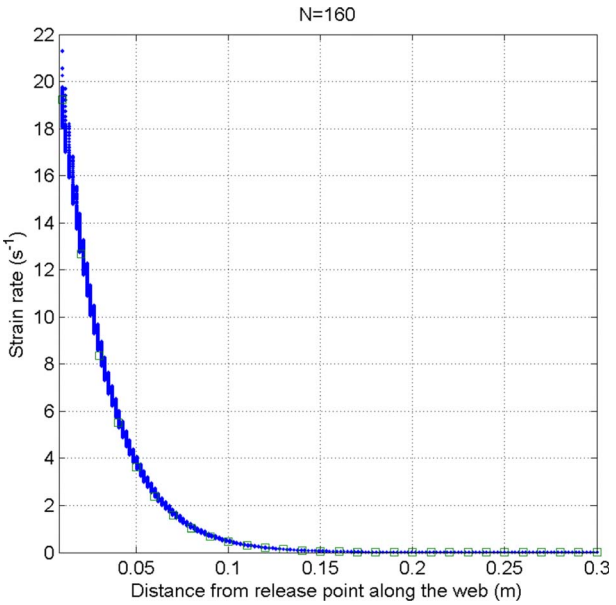

Fig. 9 The strain rate $\dot{\varepsilon}$ in the open-draw with $N=160$ nodes. The continuum result is shown as squares: $\dot{\varepsilon}(x)=k(v_2-v_1)\times[e^{-kx}/(1-e^{-kL_w})]$; $\nu=30$ m^2/s.

the sheet is $W=8.6$ m. The machine speed $v_2=1400$ m/min and draw$=(v_2-v_1)/v_1=3\%$. We estimated Young's modulus to be $E=3.5\times10^7$ Pa, which corresponds to $E^*=E/\rho=30{,}000$ N m/kg. This can be compared with literature values $E^*=22{,}500$ N m/kg [1] and $E^*=35{,}000$ N m/kg [10]. The steel roll adhesion parameter is $W_a'=7.8$ J/m^2 (from Fig. 5) and for the second roll we assume $W_a'=\infty$, so that the web will never be released again. The kinetic viscosity was estimated to be $\nu=10$ m^2/s. This can be compared with typical values of $\nu=5-30$ m^2/s [10]. The length between rolls $L=1.38$ m, $r_1=0.8$ m, $r_2=0.5$ m, and the machine orientation with respect to gravity $\theta=13.5$ deg; see Fig. 1. This makes the initial straight web length $L_w(0)=0.463$ m.

3.1 Steady-State Solutions. In Fig. 8 we display the strain along the paper web. We applied the above control parameters with the exception of the kinetic viscosity $\nu=30$ m^2/s. In this case we obtain a simple steady-state solution in the case of a homogeneous paper web. Of course, starting with the initially planar web shape (Sec. 2.2) results in a time-dependent behavior until the correct steady-state web shape is obtained. In this example this took less than 0.05 s. The simulation lasted for 1 s, which was long enough to observe the full steady-state behavior. In the upper panel we see the discrete solution in the case of $N=40$ nodes. For example, the first visco-elastic element to the left (node 1) is seen to be stretched from zero strain up to its maximum of about 0.8%. The next node further increases its stretch up to about 1.4% and so on, until the total 3% strain, as controlled by the draw, is achieved. The continuum solution curve is also displayed for comparison. We see that the maximum strain of each visco-elastic element corresponds well to the continuum result. The theoretical continuum formula given in the figure legend was shown, e.g., by Kurki et al. (see p. 414 in Ref. [3]). That solution is based on the assumption of a stationary state and the boundary conditions $\varepsilon(0)=0$ and $\varepsilon(L_w)=(v_2-v_1)/v_1$. The lower panel shows the strain in the case of $N=160$ nodes. The continuum solution is plotted here as square symbols to facilitate the comparison. The two solutions are seen to be equal. Convergence properties are further discussed in the Appendix. In Fig. 9 we consider the same physical situation but instead display the strain rate $\dot{\varepsilon}$. As expected the strain rate is very high near the release point and declines rapidly on its way to the second roll where the strain is fully developed. Again it is clear that the agreement is excellent. These high strain rates can be understood when we recognize that the total time spent for the web transfer between the rolls is only about $0.3/23.33=0.013$ s. The particular shape of the web solution is also interesting to study. This can be done through a study of web curvature; see Fig. 10. There are no geometrical constraints imposed on the present solution. In the neighborhood of the release point the web is sharply bent, and as it

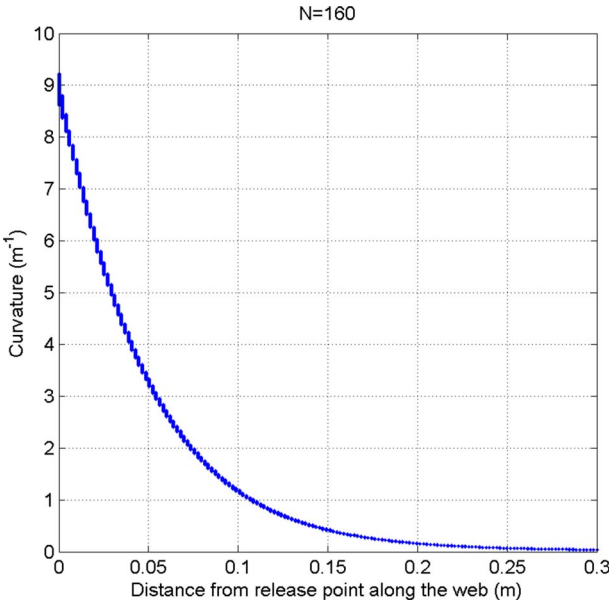

Fig. 10 The curvature κ_i (or $\kappa(x)$) in the open-draw with $N=160$ nodes. $\kappa_i\equiv1/R_i\approx2\cos(\gamma_i/2)/a_0$.

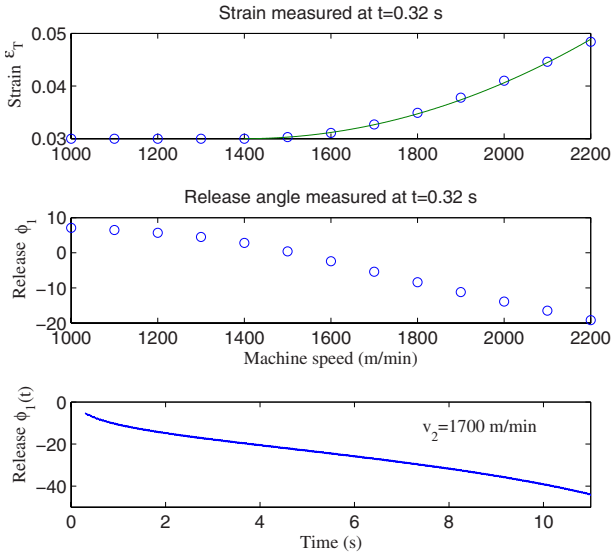

Fig. 11 ***N*=40. (Top) Total strain at *t*=0.32 s for various machine speeds. The fitted continuous curve is quadratic in speed. (Middle) The corresponding release angle ϕ_1 in deg after 0.32 s. (Bottom) For v_2=1700 m/min (and above) the release angle ϕ_1 is transient.**

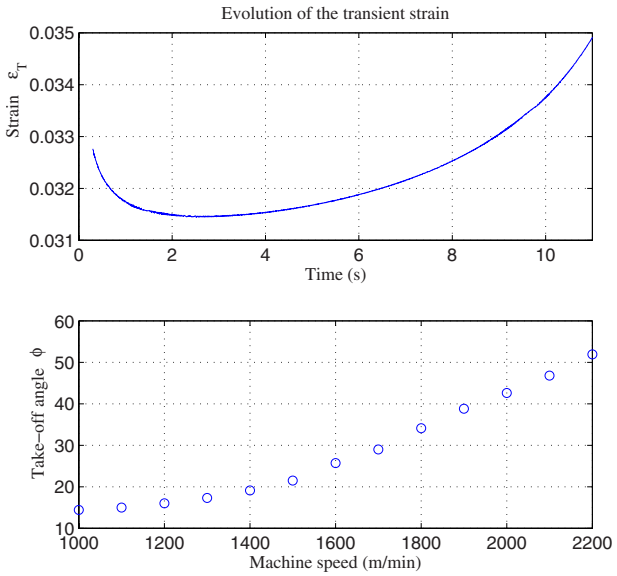

Fig. 12 ***N*=40. (Top) Strain evolution at a machine speed of 1700 m/min. (Bottom) The take-off angle ϕ recorded at *t*=0.32 s (in deg) as a function of machine speed. ϕ is calculated between the tangent line of the release point and a line intersecting a point 25% of L_w (effectively where the web is straight). Also compare with Fig. 1.**

approaches the second roll, almost a straight web geometry is seen. This general behavior is expected for a steady-state solution. However, the detailed solution is highly dependent on factors such as machine speed, mass density, elastic constant, adhesion strength, etc.

3.2 Transient Solutions. As the physical parameters are changed away from the "controlled" parameter set, situations may arise where the steady-state solution can no longer be guaranteed. As we have indicated in Secs. 2.7 and 2.8, the release conditions of the web depend on the solution itself. In particular, the release angle ϕ_1 (Fig. 1) on the first roll might become time-dependent. This is obviously the case if we introduce external time-dependent perturbations, such as roll speed variations (draw), system vibrations, aerodynamic effects, variation in adhesion strength, variations in paper material properties (moisture, mass density, elastic constant, bending stiffness, and thickness), etc. However, first, we shall investigate the effects on the web strain by testing several machine speeds v_2.

Figure 11 shows the total strain ε_T (strain in the last node) of the web recorded after 0.32 s as a function of various machine speeds. Note that each of the simulations is performed for a constant machine speed v_2 and we also keep the draw and all other parameters constant. The top panel shows that for the lower speeds we have the steady-state solution so that ε_T is always 3%. However, beyond 1500 m/min, the strain starts to grow as the machine speed increases. At the same time in the middle panel we see that the point of release is moved further and further down in the first roll. The bottom panel shows the subsequent evolution of ϕ_1 for the case of v_2=1700 m/min. The release point is moving downwards and consequently the length of the paper web within the open-draw section increases, so more and more mass are added. There is also a web curvature present leading to centrifugal forces. Intuitively, the combined effects of more mass and centrifugal forces should influence the strain. This is indeed demonstrated in Fig. 12 (top). At a machine speed of 1700 m/min, the web adjusts its geometry up to about t=3 s. That is, the system is trying to restore the steady-state strain of 3% (self-stabilizing effect). These self-adjustments of the curvature and the take-off angle ϕ (and also release angle ϕ_1) tend to keep the web tension nearly constant (see, e.g., pp. 415–418 in Ref. [3]). However, due to the web accumulation and centrifugal forces, the strain eventually starts to increase after t=3 s, as seen in Fig. 12. In the lower part of Fig. 12 we also display a snapshot of the take-off angles recorded at t=0.32 s at various speeds. The take-off angle steadily increases with machine speed. It should also be noted that at above 1600 m/min the take-off angle is transient (increases with time).

Our simulations showed that transient behavior also occurs if the density of the wet web is increased, Young's modulus is decreased, the adhesion strength is increased, the paper thickness is decreased, or the draw is too small. We have also investigated the effect of changing the distance L between rolls (Fig. 1) in order to see if the effect of centrifugal forces declines. However, almost an identical strain dependence on machine speed was observed as that in Fig. 11 (top). The length and curvature of the web adjust to the new situation so they become nearly the same. From this point of view the effect of changing L is insignificant.

3.3 External Perturbations. In this section we demonstrate the effect of external perturbations by a certain decline in Young's modulus or an increase in basis weight occurring in the incoming paper web at the first roll. This could, for example, happen if the wetness of the paper web increases. With regard to the maximum strain in the web it is not necessary to plot $\varepsilon(x,t)$ along every web location x. Instead we simply study $\varepsilon_T(t)$, i.e., the strain near the second roll. In steady-state operation this is the position where the strain is at maximum (Fig. 8). For the transient solutions (time-dependent ϕ_1, web curvature, and web length) in this section, we have computed $\max(\varepsilon(x,t))$ at each instant of time and it was found that $\max(\varepsilon(x,t))=\varepsilon(L_w,t)\equiv\varepsilon_T(t)$ still holds.

At t=5 s each node that enters the open-draw has a 15% lower stiffness; see Fig. 13. Since the time required for the web to travel from the first roll to the second roll is only about 10 ms, the response in the strain is fast. At t=5 s the strain surges up to almost 3.5%, and then the web attempts to adjust itself to the new condition lowering the strain to about 3.35%. This perturbation together with the quite high machine speed (1600 m/min) then makes the solution transient. However, at t=8 s, when the elastic

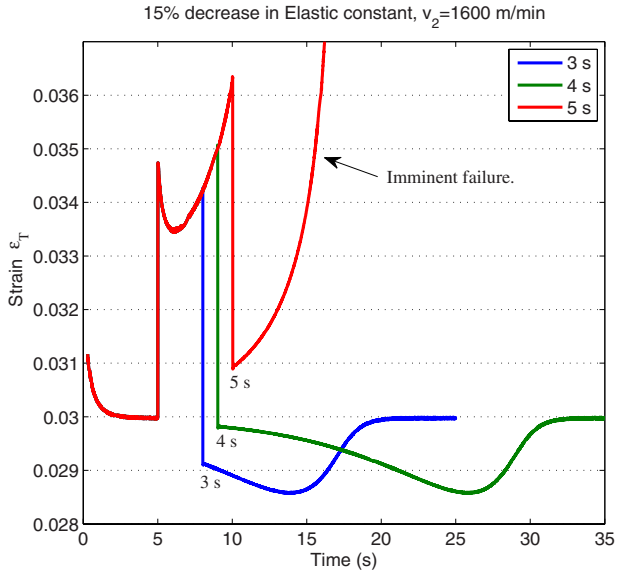

Fig. 13 Total strain ε_T (i.e., strain at the last node) as a function of time. The elastic constant is decreased by 15% at $t=5$ s. The durations (3 s, 4 s, and 5 s) are then studied after which the elastic constant is restored. $N=40$.

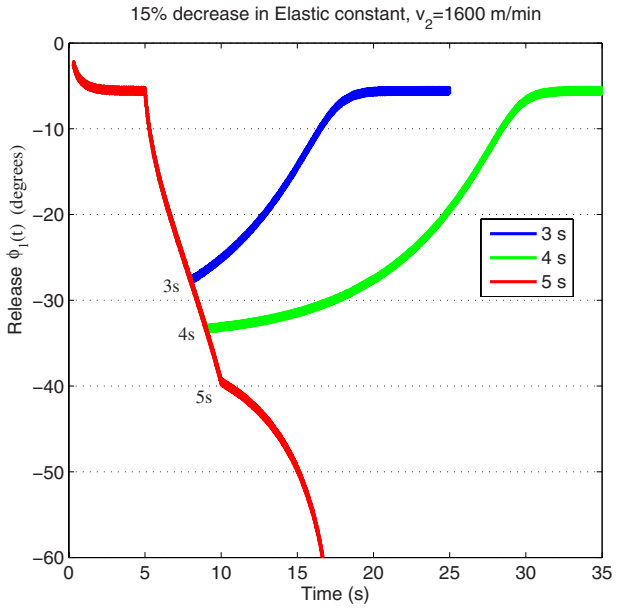

Fig. 14 The corresponding evolution of the release angle $\phi_1(t)$ for the cases in Fig. 13. $N=40$.

constant is restored to its original value, the strain temporarily decreases to 2.9%. Finally at $t=20$ s the steady-state solution is restored and the strain becomes 3%.

It is interesting to examine if the duration of the perturbation has any impact on this behavior. The first curve in Fig. 13 discussed above was for a 3 s duration. The next curve is the result for a 4 s duration, where essentially the same features are observed, except that it takes longer time for the steady-state to be restored. However, in the last case, with a duration of 5 s, a different behavior can be seen. After the stiffness has been restored at $t=10$ s, the strain continuously grows without any sign of recovery, and thus web failure is imminent.

This instability behavior may be interpreted as follows. At $t=5$ s, a 15% softer paper web starts to enter the open-draw. In only about 10 ms the whole open-draw has been replaced with the softer web. Due to the lower elastic stiffness there is a rapid response in the strain ε_T resulting in a surge to almost 0.035. The paper web then starts to adjust to the new situation by decreasing the release angle ϕ_1 (Sec. 2.8), increasing the web length in the open-draw section, changing the web curvature, resulting in an initial relaxation of the strain. However, during this process, the web curvature near the first roll continues to grow (resulting in increased stress due to centrifugal forces) and the length of the web becomes longer as well (more stress due to gravity). Eventually the strain therefore starts to increase until $t=10$ s at which the elastic stiffness is restored. Due to the stiffer paper web the strain decreases rapidly. However, the web is still sharply bent and remains long. These conditions, again, lead to an increasing strain and a continuous decrease in the release angle ϕ_1, as is also seen in Fig. 14. Here we see how ϕ_1 responds to the changes in stiffness. In the first two cases ϕ_1 eventually returns to the initial steady-state value, while in the last case, the continuous decrease in ϕ_1 is seen. It is thus predicted that dangerously high strain levels of the paper web will be reached in the last case.

Figure 15 is another example where an increase in grammage (either by fiber or water) is introduced for certain time durations. After a short transient behavior from the start of the simulation, the strain ε_T reaches its equilibrium value of 3% (which equals the draw κ). At $t=5$ s, the grammage ($g=\rho T$) is gradually increased by 15% according to $g(t-t_i)=g_0e^{-\tau(t-t_i)}$, where t_i is the time when the perturbation starts ($t_i=5$ s), g_0 is the original grammage (unperturbed), and τ is chosen such that when $t=t_f=7$ s, the grammage is increased by 15%. After $t=t_f$, the grammage is kept constant ($=1.15g_0$). At the end of the perturbation the grammage is gradually restored (corresponding to a 50 m paper web). This gradual restoration is made similarly as above but instead with an exponential decline during 2 s. For the durations of 6 s and 7 s (Fig. 15), the strain ultimately restores to its initial value of 3%. However, the transient behavior becomes irreversible after 8 s: Steady-state operation is not restored. In other words the duration of the perturbation is critically important. Besides an increased grammage, the transient behavior can also be triggered by an increase in adhesion strength (not shown).

Figure 16 displays the imminent solution in Fig. 13, but with

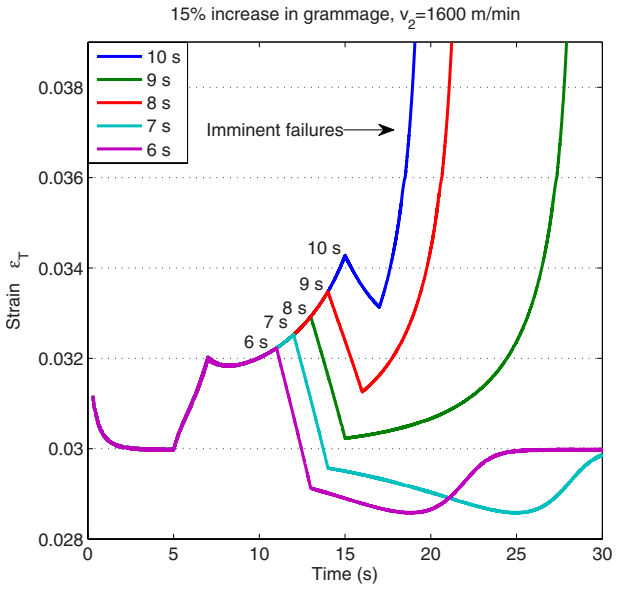

Fig. 15 Total strain ε_T as a function of time. The grammage of the paper web entering the open-draw gradually increases to 15% during $t=5-7$ s. This perturbation is maintained for the durations 6 s, 7 s, 8 s, 9 s, and 10 s after which the original grammage is restored gradually during 2 s. $N=40$.

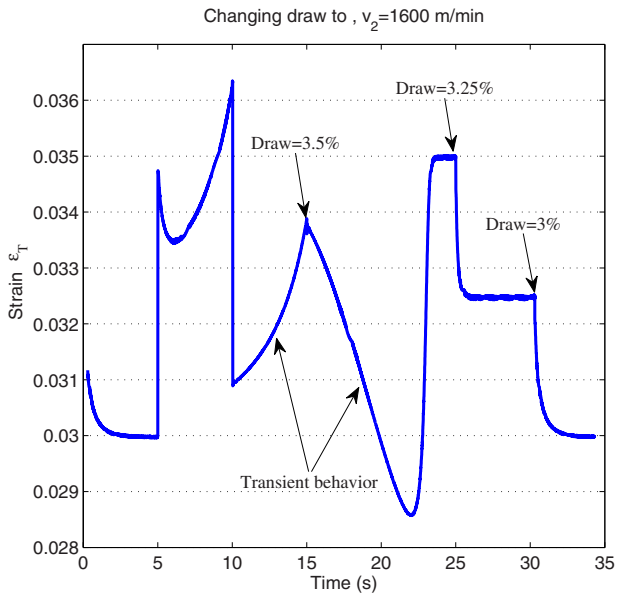

Fig. 16 Total strain as a function of time. Changing the draw at strategical timings is shown to be beneficial. $N=40$.

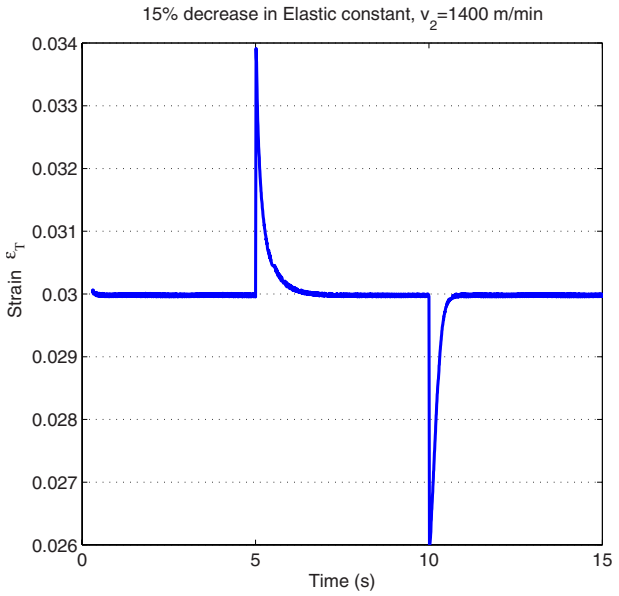

Fig. 17 The strain response to the elastic modulus perturbation. The perturbation was given between 5 s and 10 s, similar to the case in Fig. 13. After the perturbation is turned on at $t=5$ s, the web quickly adjusts to a new curvature, ϕ and ϕ_1, and the steady-state strain of 3%. As the perturbation is turned off at $t=10$ s, the web strain temporarily decreases and then returns to steady-state. $N=40$.

some examples of countermeasures by allowing various levels of the draw. After $t=15$ s when the transient solution is growing we increase the draw to 3.5%. This stops the imminent solution. The web solution is still time-dependent, but approaches the steady-state strain at about $t=23$ s. At $t=25$ s the draw is changed into 3.25% and a smooth transition to the new level is soon accomplished. At $t=30$ s we restore the draw to its original level of 3% and, again, a smooth transition takes the solution back to its original steady-state and strain level at 3%. In practice this countermeasure may not be feasible because the draw might fluctuate in itself during normal operation (see, e.g., in the printing press [9]).

In Fig. 17 we plot a similar perturbation as in Fig. 13 but with a machine speed of only 1400 m/min. In this case the imminent behavior is not triggered. When the elastic constant is decreased by 15% at $t=5$ s, a fast surge in strain occurs up to 3.4% but then a smooth transition takes place to restore the steady-state of 3% strain. At $t=10$ s the elastic constant is restored. Here the strain immediately drops and then smoothly returns to the steady-state. This situation is clearly distinct from the previous case (Fig. 13) where the same perturbation brought the system to a complete break down. We also note that the time spent with dangerously high strain is much shorter in Fig. 17. Also similar behavior was obtained for other perturbations, such as an increase in web mass density, adhesion strength, etc.

4 Conclusions and Further Work

We have developed a novel model to investigate the system dynamics of the open-draw section. In spite of its simple treatment, the model represented numerous advantages over the conventional approaches, and could display rich phenomena of nonlinear dynamics of the open-draw. For example, it is advantageous that the web solution is not constrained by any particular shape and can fully take into account the dynamic boundary conditions derived from the physical situation. The model is flexible enough to study the effect of variations in mass density, elastic stiffness, viscous effects, paper thickness, draw, system geometry, etc. The critical importance of the release point and its sensitivity to both system and material variations was recently pointed out in Ref. [4]. In fact, the present work has confirmed these observations and clarified further implications of the transient behavior. For example, despite the lack of external perturbations, the solution can still be time-dependent (i.e., steady-state cannot be obtained for certain parameters). The boundary conditions depend on the solution itself. This complication can lead to a dangerous situation for a certain set of parameters. Some examples are a decrease in elastic constant or an increase in mass density. This is consistent with an increasing moisture content of the paper web. A high adhesion strength, low thickness, or a too small draw can also trigger transient behavior.

In this work we left out some important effects. One approximation is that slippage between a roll surface and the web is not considered. If this happens, prestrain can build up and becomes added to the existing strain, which could then induce dangerous situations. Due to the nonlinearity of the solutions one could expect chaotic behavior to occur in some solutions. It would also be very interesting to perform simulations beyond the 1D paper web. However, the number of visco-elastic parameters implied by a 2D paper web grows considerably [36], and, as a consequence, difficulties may arise in order to establish precise input parameters. Also, the computational complexity of the calculations grows. In order to limit the volume of the present work, the above considerations are left for future studies.

Acknowledgment

The authors are grateful to Dr. S. Lindström and Professor P. Gradin for many valuable discussions. The authors wish to thank SCA R&D in Sundsvall and Stora Enso Falun Research Centre for valuable inputs. Financial support from the KK-foundation and the European structural funds are greatly acknowledged.

Appendix

1 Particle Approach and Phonon Waves. In the paper it is claimed that a particle system can mimic the corresponding continuum mechanical solution for a beam (with axial and bending responses). Although this may be intuitively clear for most readers, it may still be worthwhile to make some comments on this. The most straightforward way is to consider phonons as given in condensed matter theory. This description is considered valid at all scales. The continuum approximation then corresponds to con-

Table 1 Richardson extrapolation [23] for a beam with length $L=0.1$ m. The beam is initially compressed with $\varepsilon=0.25$. All values are in SI-units. $\Delta=F_x(a_0/2)-F_x(a_0)$. The ratios in col. 4 equal 4 (2^{p_1}), so $p_1=2$ and in col. 6, 16 so $p_2=4$. $\hat{F}_x$ and $\hat{\hat{F}}_x$ denote extrapolated values.

N	a_0	$F_x(a_0)$	$\Delta/(2^{p_1}-1)$	$\hat{F}_x$	$\Delta/(2^{p_2}-1)$	$\hat{\hat{F}}_x \approx F_x(0)$
11	0.01	0.028125722	-	-	-	-
21	0.005	0.028301356	5.854467×10^{-5}	0.02835990	-	-
41	0.0025	0.028345385	1.467633×10^{-5}	0.02836006	1.067×10^{-8}	0.02836007
81	0.00125	0.028356400	3.67167×10^{-6}	0.02836007	6.7×10^{-10}	0.02836007

sidering waves with long wavelengths much larger than the distance a between atoms. In order to keep this presentation as clear as possible we shall assume a homogeneous system.

Consider two 1D lattice grids: I and II, one with spacing a_{I} (atomic scale) and one with spacing $a_{\mathrm{II}}=xa_{\mathrm{I}}$, where $x\geq1$ is an integer. In this case we consider waves with $\lambda\gg xa_{\mathrm{I}}$, say, $\lambda=xya_{\mathrm{I}}$, where $y\gg1$ is a real number. We adopt the 1D phonon approach in solid state physics, e.g., Ref. [37], where a phonon wave is written as

$$u_s = Ae^{iska}e^{-i(\omega t-\delta)}$$

where a node of the lattice is denoted by the integer s, k is the wave vector, and the phase factor δ is determined from the initial condition of the wave. The angular frequency ω is given by

$$\omega = 2\sqrt{\frac{C}{m}}\left|\sin\frac{ka}{2}\right|$$

Thus in the first lattice we have that $ka_{\mathrm{I}}=2\pi/xy$ so $\omega_{\mathrm{I}}=2\sqrt{C_{\mathrm{I}}/m_{\mathrm{I}}}|\sin(\pi/xy)|\approx2\pi/xy\sqrt{C_{\mathrm{I}}/m_{\mathrm{I}}}$, since $xy\gg1$. In the second lattice we have that the mass of an effective particle $m_{\mathrm{II}}=xm_{\mathrm{I}}$ (to conserve mass density) and the effective stiffness is $C_{\mathrm{II}}=C_{\mathrm{I}}/x$. In this case $ka_{\mathrm{II}}=kxa_{\mathrm{I}}=2\pi/y$. Thus $\omega_{\mathrm{II}}=2\sqrt{C_{\mathrm{II}}/m_{\mathrm{II}}}|\sin(\pi/y)|=2/x\sqrt{C_{\mathrm{I}}/m_{\mathrm{I}}}|\sin(\pi/y)|\approx2\pi/xy\sqrt{C_{\mathrm{I}}/m_{\mathrm{I}}}$, so $\omega_{\mathrm{I}}=\omega_{\mathrm{II}}$. The only difference between the waves $u_s(\mathrm{I})=Ae^{is_{\mathrm{I}}ka_{\mathrm{I}}}e^{-i(\omega_{\mathrm{I}}t-\delta)}$ and $u_s(\mathrm{II})=Ae^{is_{\mathrm{II}}ka_{\mathrm{II}}}e^{-i(\omega_{\mathrm{II}}t-\delta)}$ is in the spatial factors $s_{\mathrm{I}}ka_{\mathrm{I}}$ and $s_{\mathrm{II}}ka_{\mathrm{II}}(=s_{\mathrm{II}}kxa_{\mathrm{I}})$. However, suppose the lattice is of length $L=Ma_{\mathrm{I}}$, where M is an integer. Then $s_{\mathrm{I}}=1,2,\ldots,M$. In the second lattice $L=Ma_{\mathrm{I}}=Ma_{\mathrm{II}}/x$ so $s_{\mathrm{II}}=1,2,\ldots,M/x$. For well chosen lattices we see that for every integer s_{II} there is a corresponding integer s_{I} such that $s_{\mathrm{II}}=s_{\mathrm{I}}/x$. Thus $s_{\mathrm{I}}ka_{\mathrm{I}}=s_{\mathrm{II}}ka_{\mathrm{II}}$ and the waves in the two lattices are, in fact, identical.

2 Particle Approach and Buckling. It is interesting to test that the bending model given in Sec. 2.4 indeed corresponds well to the continuum model of a buckling beam (e.g., Ref. [38]). It is also worthwhile to study the convergence properties with regard to the number of particles utilized in the model. We set up a numerical experiment with the same reference parameters as in Sec. 3. We first place N particles along an arbitrary axis, say, the x-axis. The particles are all separated by a certain distance $a=(1-\varepsilon)a_0$ (i.e., the compressed system). At all times we keep the particles 0 and $N-1$ fixed. Then we introduce a small transverse perturbation ($y=10^{-14}$ m) in the central particle ($y=0$ for the rest). The system will then naturally relax ($a\rightarrow a_0$) and converge into a bent beam due to the imposed damping. The longitudinal force F_x acting on particle 0 is tabulated in Table 1. F_x is a function of the number of utilized particles N (or a_0). In the case of a large deflection there is no analytic formula for the continuum limit $F_x(a_0\rightarrow0)$. Given the lattice separations a_0 in Table 1 and the standard properties of extrapolation [23], we find that $F_x(0)=F_x(a_0)+2.35a_0^2+\mathcal{O}(a_0^4)$. The convergence is quadratic and thus fast. A corresponding experiment with a compression of only $\varepsilon=0.05$ results in $F_x(0)=F_x(a_0)+2.08a_0^2+\mathcal{O}(a_0^4)$, where in this case $F_x(0)=0.025393$ N, which can be compared with the approximation $F_x(0)=\pi^2ET^3W/12L^2=0.024756$ N [38] (valid only for a small deflection). This limit corresponds to an extremely small compression, namely, $\varepsilon=\pi^2T^2/12L^2$. Given $F_x(0)$, the exact relation for the continuous beam is [38]

Table 2 Richardson extrapolation [23] of the beam property $K=yR$. All values are in SI-units. $\Delta=K(a_0/2)-K(a_0)$. The ratios in col. 4 equal 4 and thus $p_1=2$. $\hat{K}$ denotes the extrapolated value.

N	a_0	$K(a_0)$	$\Delta/(2^{p_1}-1)$	$\hat{K}\approx K(0)$
11	0.01	8.958637×10^{-4}	-	-
21	0.005	8.87291×10^{-4}	-2.857×10^{-6}	8.8443×10^{-4}
41	0.0025	8.85158×10^{-4}	-7.110×10^{-7}	8.8445×10^{-4}
81	0.00125	8.84632×10^{-4}	-1.775×10^{-7}	8.8446×10^{-4}

$$yR = \frac{ET^3W}{12F_x(0)} \tag{A1}$$

where y is the transverse displacement of the beam and R is its corresponding radius of curvature (at that position). According to Eq. (A1), the continuum value is given by $yR=8.8446\times10^{-4}$ m^2 for $\varepsilon=0.25$. From the numerical experiment we also recorded y and R for the center particle. This is tabulated in Table 2. We see that the extrapolated value indeed equals the continuum value. In the case of $\varepsilon=0.05$ the continuum result is $yR=9.878\times10^{-4}$ m^2, which again agrees with the extrapolated value (not shown). We conclude that there is a direct correspondence between the particle picture and the continuum picture, and, in fact, already at $N=40$, they are very similar.

References

[1] Wahren, D., 1981, "Wet Webs in Open Draws—An Engineering Analysis," Tappi J., **64**, pp. 89–93.
[2] Seth, R. S., Barbe, M. C., Williams, J. C. R., and Page, D. H., 1982, "The Strength of Wet Webs—A New Approach," Tappi J., **65**, pp. 135–138.
[3] Kurki, M., Pakarinen, P., Juppi, K., and Martikainen, P., 2000, *Drying–Papermaking Part 2*, Finnish Paper Engineers' Association, Helsinki.
[4] Makinen, J. T., 2004, "Multi-Variable Controls," Automation, **2**, pp. 4–7.
[5] Mardon, J., Truman, A. B., O'Blenes, G., and Meadley, K., 1958, "A Consideration of the Factors Involved at the Open Draw at Couch and Presses of Fourdrinier Machines," Pulp and Paper Magazine of Canada, Sept., pp. 135–155.
[6] Österberg, L., 1962, "Pappersbanors avtagning från pressvalsar," Sven. Papperstidn., **65**, pp. 222–233.
[7] Mardon, J., 1976, "Theoretical and Experimental Investigations Into Peeling of Paper Webs From Solid Surfaces," Papper och Trä, **11**, pp. 797–815.
[8] Gavelin, G., 1958, "The Case of the Open Draw," Sven. Papperstidn., **61**, pp. 282–286.
[9] Hristopulos, D. T., and Uesaka, T., 2002, "A Model of Machine-Direction Tension Variations in Paper Webs With Runnability Applications," J. Pulp Pap. Sci., **28**, pp. 389–394.
[10] Kurki, M., Vestola, J., Martikainen, P., and Pakarinen, P., 1997, "The Effect of Web Rheology and Peeling on Web Transfer in Open Draw," *1997 Proceedings of the Fourth International Conference of Web Handling*, p. 527.
[11] Ahrens, F., Patterson, T., and Bloom, F., 2004, "Mathematical Modelling of Web Separation and Dynamics on a Web Adhesion and Drying Simulator," Int. J. of Applied Mechanics and Engineering, **9**, pp. 227–271.

[12] Frenkel, D., and Smit, B., 2002, *Understanding Molecular Simulation*, 2nd ed., Academic, New York.
[13] Ostoja-Starzewski, M., 2008, *Microstructural Randomness and Scaling in Mechanics of Materials*, Chapman and Hall, London/CRC, New York, p. 157.
[14] Li, S., and Liu, W. K., 2002, "Meshfree and Particle Methods and Their Applications," Appl. Mech. Rev., **55**, pp. 1–34.
[15] Cundall, P. A., and Strack, O. D. L., 1979, "Discrete Numerical-Model for Granular Assemblies," Geotechnique, **29**, pp. 47–65.
[16] Reeves, W. R., and Greenspan, D., 1982, "An Analysis of Stress Wave-Propagation in Slender Bars Using a Discrete Particle Approach," Appl. Math. Model., **6**, pp. 185–191.
[17] Monaghan, J. J., 1982, "Why Particle Methods Work," SIAM (Soc. Ind. Appl. Math.) J. Sci. Stat. Comput., **3**, pp. 422–433.
[18] Meguro, K., and Tagel-Din, H., 2001, "Applied Element Simulation of RC Structures Under Cyclic Loading," J. Struct. Eng., **127**, pp. 1295–1305.
[19] Schiehlen, W., 2007, "Research Trends in Multibody System Dynamics," Multibody Syst. Dyn., **18**, pp. 3–13.
[20] Etzmuss, O., Gross, J., and Strasser, W., 2003, "Deriving a Particle System From Continuum Mechanics for the Animation of Deformable Objects," IEEE Trans. Vis. Comput. Graph., **9**, pp. 538–550.
[21] Lloyd, B. A., Szekely, G., and Harders, M., 2007, "Identification of Spring Parameters for Deformable Object Simulation," IEEE Trans. Vis. Comput. Graph., **13**, pp. 1081–1094.
[22] Goldstein, H., 1980, *Classical Mechanics*, 2nd ed., Addison-Wesley, Reading, MA, p. 545.
[23] Burden, R. L., and Faires, J. D., 1989, *Numerical Analysis*, 4th ed., PWS-Kent, p. 157.
[24] Birkhoff, G., and Rota, G. C., 1978, *Ordinary Differential Equations*, 3rd ed., Wiley, New York, p. 126.
[25] Barzanti, L., Corradi, C., and Nardon, M., 2006, "On the Efficient Application of the Repeated Richardson Extrapolation Technique to Option Pricing," Working Paper Series, Department of Applied Mathematics, University of Venice.
[26] Smith, M. C., 2002, "Synthesis of Mechanical Networks: The Inerter," IEEE Trans. Autom. Control, **47**, pp. 1648–1662.
[27] Landau, L. D., and Lifshitz, E. M., 1986, *Theory of Elasticity*, 3rd ed., Reed Educational and Professional Publishing Ltd., pp. 64–67.
[28] Rivlin, R. S., 1944, "The Effective Work of Adhesion," Paint Technol., **9**, pp. 215–216.
[29] Kaelble, D. H., 1959, "Theory and Analysis of Peel Adhesion: Mechanisms and Mechanics," J. Rheol., **3**, pp. 161–180.
[30] Nicholson, D. W., 1977, "Peel Mechanics With Large Bending," Int. J. Fract., **13**, pp. 279–287.
[31] Mardon, J., 1961, "The Release of Wet Paper Webs From Various Papermaking Surfaces," Appita J., **15**, pp. 14–34.
[32] Wang, X., 1997, "Finite Element Analysis of Air-Sheet Interactions and Utter Suppression Devices," Comput. Struct., **64**, pp. 983–994.
[33] Pramila, A., 1986, "Sheet Utter and the Interaction Between Sheet and Air," Tappi J., **69**, pp. 70–74.
[34] Blevins, R. D., 1990, *Flow-Induced Vibration*, Van Nostrand Reinhold, New York, p. 1.
[35] Chang, Y. B., and Moretti, P. M., 1991, "Interaction of Fluttering Webs With Surrounding Air," Tappi J., **74**, pp. 231–236.
[36] Sato, J., Hutchings, I. M., and Woodhouse, J., 2007, *Proceedings of the 61st Appita Annual Conference and Exhibition*, Gold Coast, Australia, Apr. 6–9, p. 15.
[37] Kittel, C., 1996, *Introduction to Solid State Physics*, 7th ed., Wiley, New York, p. 99.
[38] Feynman, R. P., 1989, *The Feynman Lectures on Physics*, Vol. II, Addison-Wesley, Reading, MA, pp. 38–11.